Electronic Supplementary Material (ESI) for Nanoscale.

Supporting information

Boosting the efficiency of transient photoluminescence microscopy using cylindrical lenses

*Alvaro J. Magdaleno,[a] Mercy M. Cutler,[a] Jesse J. Suurmond,[a] Marc Meléndez,[b] Rafael Delgado-Buscalioni,[b] Michael Seitz,[a] Ferry Prins[a]**

a. Condensed Matter Physics Center (IFIMAC) and Department of Condensed Matter Physics, Universidad Autónoma de Madrid, 28049 Madrid, Spain.

b. Condensed Matter Physics Center (IFIMAC) and Department of Theoretical Condensed Matter Physics, Universidad Autónoma de Madrid, 28049 Madrid, Spain.

Experimental methods

2D perovskite preparation

Perovskite solutions were made in a N_2-filled glovebox following the recipes given in refs.[1–3] In short, n = 1 phenethylammonium lead iodine $(PEA)_2PbI_4$ solutions were prepared by mixing stoichiometric ratios of the precursor salts. Phenethylammonium iodide (PEAI) (Sigma Aldrich, 805904-25G) and lead(II) iodide (PbI_2) (Sigma Aldrich, 211168-50G) were mixed with a stoichiometric ratio of 2:1 and dissolved in anhydrous n,n-dimethylformamide (DMF, Sigma Aldrich, 227056-1L). The solution was heated to 70°C while stirring until all the precursors were completely dissolved. The resulting solution was kept at 70°C and the solvent was left to evaporate until reaching saturation of the solution.

Perovskite crystals (hundreds of micron lateral sizes) were obtained using drop casting of the saturated perovskite solution on top of a microscope slide and heating to 50°C for 2-3 hours until drying. The perovskite crystals of the thin film were mechanically exfoliated using the Scotch tape (Scotch Magic) method. After several exfoliation steps, the crystals were transferred on a glass slide and were subsequently studied through the glass slide with a ×100 oil immersion objective (Nikon CFI Plan Fluor, NA = 1.3).

CdSe QD samples

CdSe/ZnS (Sigma Aldrich, 790192) thin films are made to carry out the measurements. The surface functionalization of octadecyltrichlorosilane (OTS, Sigma Aldrich, 104817-25G) based self-assembled monolayers explained by Prins, et al[4] is applied to increase the hydrophobicity of the glass substrates (24x24x0.16 mm, Labbox, COVN-024-200). It is needed to get smooth and densely packed QD films for the diffusion measurements. For safety reasons, the surface functionalization process of Prins, et al[4] is slightly modified, using a plasma treatment instead of the piranha cleaning for the generation of the oxygen radicals in the glass surface. The plasma cleaning was applied during 1 min, the chosen gas to create the plasma was air.

CdSe/ZnS solutions of ~40 mg/mL[5] are prepared using a hexane:octane ratio of 9:1. Subsequently, the QD solutions are drop casted on the functionalized glass substrates.

Emission profile measurements

The materials were excited with a 405 nm laser (PicoQuant LDH-D-C-405, PDL 800-D), which was focused down to a near diffraction limited spot. The laser spot images were acquired using an EMCCD camera coupled to a spectrograph (Princeton Instruments, SpectraPro HRS-300, ProEM HS 1024BX3) with a x430 magnification for the spherical and x430 (y-axis), x32 (x-axis) for the cylindrical lenses configuration, i.e. 100x oil immersion objective with the additional magnification of the respective lenses. Results are shown in **Figure 2**.

Exciton propagation length

Fluorescence lifetime measurements were performed using a laser diode of λ = 405 nm (PicoQuant LDH-D-C-405, PDL 800-D, Pico-Harp 300) and an avalanche photodiode (APD, Micro Photon Devices PDM). The repetition rate was 40 MHz and the peak fluence per pulse was 50 nJ cm^{-2}. **Figure S5** shows the photoluminescence lifetime traces of the 2D perovskites and CdSe QDs and the fit parameters of a bi-exponential fit to the data. The fit was used together with the experimentally obtained time-dependent MSD to extract the total number of surviving excitons for a given time t as presented in **Figure S6**. The exciton propagation length is defined as the net distance at which 1/e of the free excitons remain. The total number of surviving excitons at time t is given by:

$$\text{surviving excitons (t)} = \frac{\int_t^\infty w_1 e^{-\frac{t}{\tau_1}} + w_2 e^{-\frac{t}{\tau_2}} dt}{\int_0^\infty w_1 e^{-\frac{t}{\tau_1}} + w_2 e^{-\frac{t}{\tau_2}} dt}$$

Simulations of signal enhancement (I_{cyl}/I_{sph})**:**

The simulations shown in **Figure 5** were conducted for an APD size d_0 = 20 µm and a fixed y-axis magnification of M_y ~ 400. Initially, the time-integrated intensity of a Voigt(x,y) population was integrated along the APD scan area for a magnification ratio of 1 (spherical lens configuration). Subsequently, we decreased the magnification on the x-axis, resulting in the compression of the population distribution and leading to the expected intensity enhancements along the APD scan area. The magnification ratios were varied from 1 to 32, while the FWHM of the population was varied from 0.3 to 1.3 µm.

We also simulated the signal enhancements for a population with a Gaussian distribution $G(\sigma; x, y)$, being the σ^2 variance. Here, we derived a general expression of the intensity enhancement. Considering;

Projected detector width on the y-axis: $\frac{d_0}{M_y}$

Projected detector width on the x-axis: $\frac{d_0}{M_x}$

Projected detector width to population width on the y-axis: $\frac{d_0}{\sigma M_y} \equiv a_y$

Projected detector width to population width on the x-axis: $\frac{d_0}{\sigma M_x} \equiv \frac{M_y}{M_x} a_y$

To obtain the intensity enhancement, we then integrate the intensities of the population that are within the projected detector as follows:

$$\text{Signal enhancement} = \frac{\int_{-\frac{d_0}{M_x/2}}^{\frac{d_0}{M_x/2}} G(\sigma;x,y)dx}{\int_{-\frac{d_0}{M_y/2}}^{\frac{d_0}{M_y/2}} G(\sigma;x,y)dy} = \frac{\int_{-\frac{d_0}{M_x/2/\sigma}}^{\frac{d_0}{M_x/2/\sigma}} G(1;x,y)dx}{\int_{-\frac{d_0}{M_y/2/\sigma}}^{\frac{d_0}{M_y/2/\sigma}} G(1;x,y)dy}$$

By using the next property: $\int_{-\frac{a}{2}}^{\frac{a}{2}} \frac{1}{\sqrt{2\pi}} e^{-\frac{x^2}{2}} dx = \text{erf}(\frac{a}{2\sqrt{2}})$

$$\text{Signal enhancement} = \frac{\text{erf}\left(\frac{a_y M_y}{2\sqrt{2} M_x}\right)}{\text{erf}\left(\frac{a_y}{2\sqrt{2}}\right)} = \frac{\text{erf}\left(\frac{d_0}{2\sqrt{2}\sigma}\frac{1}{M_x}\right)}{\text{erf}\left(\frac{d_0}{2\sqrt{2}\sigma}\frac{1}{M_y}\right)}$$

Taking into account the next expression: $\text{FWHM} = \sigma 2\sqrt{2\ln(2)}$

$$\text{Signal enhancement} = \frac{\text{erf}\left(\frac{\sqrt{\ln(2)}}{FWHM}\frac{d_0}{M_y}\frac{M_y}{M_x}\right)}{\text{erf}\left(\frac{\sqrt{\ln(2)}}{FWHM}\frac{d_0}{M_y}\right)} \qquad (1)$$

The resulting **Ecuation 1** was used to plot_**Figure S7** (assuming $d_0 = 20$ µm and $M_y = 400$) and to plot **Figure S8** for a more general simulation, where d_0, M_x, M_y and the FWHM have been left as free parameters.

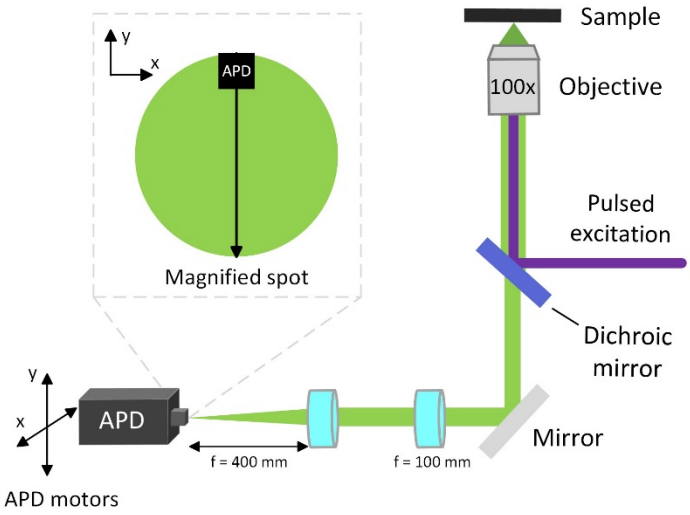

Figure S1. Conventional TPLM with spherical lenses. The sample is excited with a laser pulse. The photoluminescence spot is visualized with a x100 magnification objective. The PL light is filtered with a dichroic mirror and sent through a lens (with 100 mm focal length) and a spherical lens with a long focal length (f = 400 nm) to obtain a final magnification of around x400.

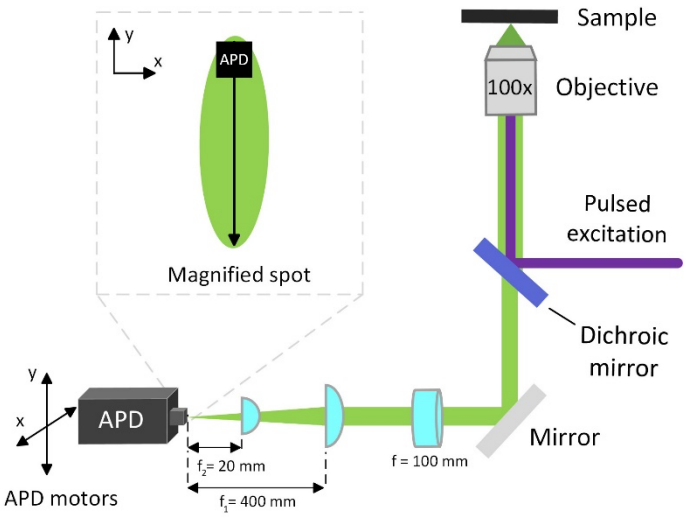

Figure S2. Optical set-up configuration with cylindrical lenses. The sample is excited with a laser pulse. The photoluminescence spot is visualized with a x100 magnification objective. The PL light is filtered with a dichroic mirror and sent through a lens (with 100 mm focal length) and a set of two cylindrical lenses. The last two project with high magnification the y-axis of the PL spot while keeping a smaller magnification on the x-axis.

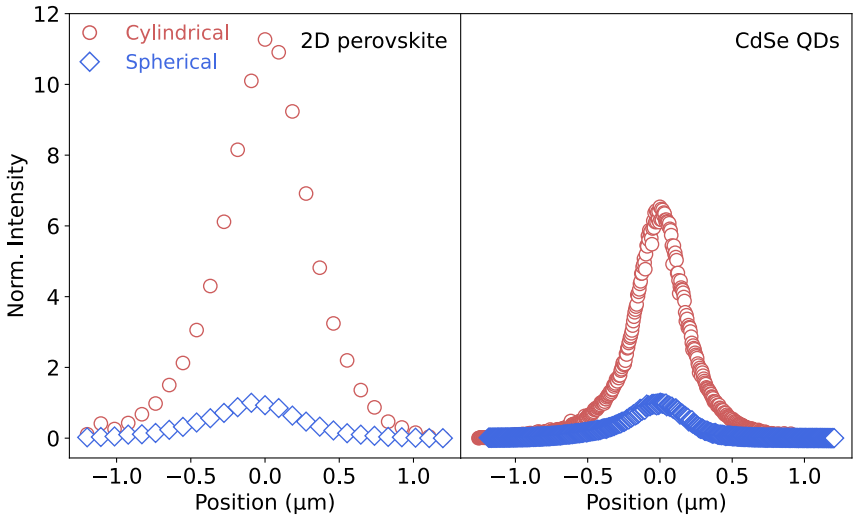

Figure S3. TPLM intensities obtained along the raster scan of the APD across the PL spot. The intensities captured with the cylindrical lenses are depicted in red and with the spherical lens in blue. For a better comparison the values are normalized to the maximum intensity measured with the spherical lens configuration.

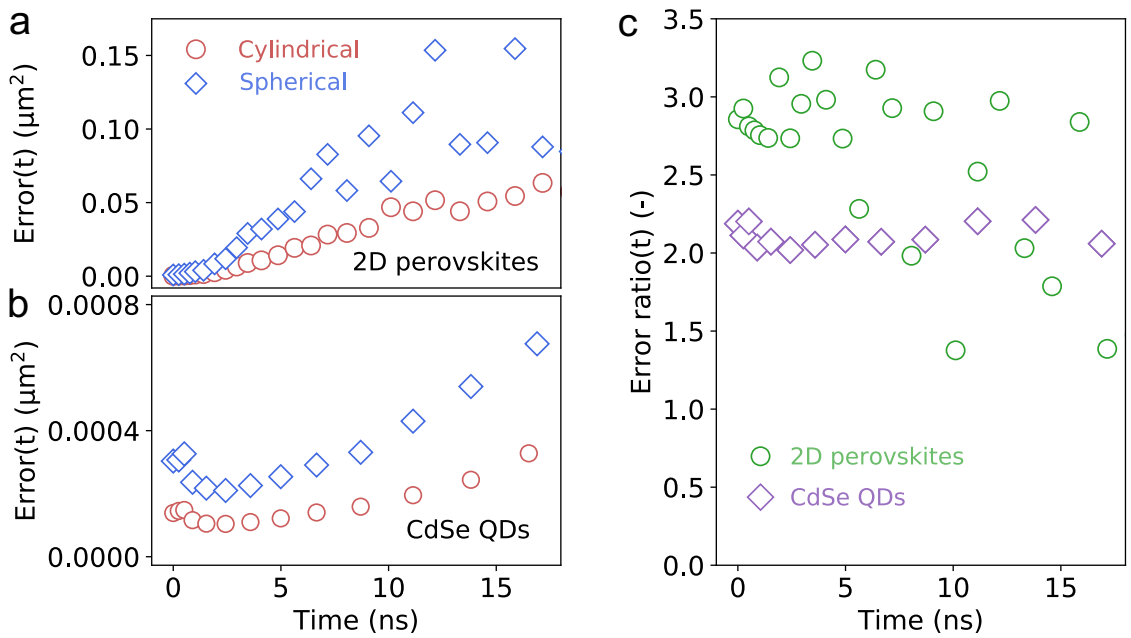

Figure S4. (a-b) Error of the $\sigma^2(t)$ values obtained from the fits to the spatial distribution at each time-slice for both the spherical (blue diamonds) and cylindrical (red circles) lens setups associated with the diffusion measurements shown in **Figure 3** (2D perovskite) and **4** (CdSe QDs), respectively. (c) Spherical vs cylindrical lens set-up error ratios. For the 2D perovskites, the error ratios are x3 (green) while in the CdSe QS are x2 (purple), approximately.

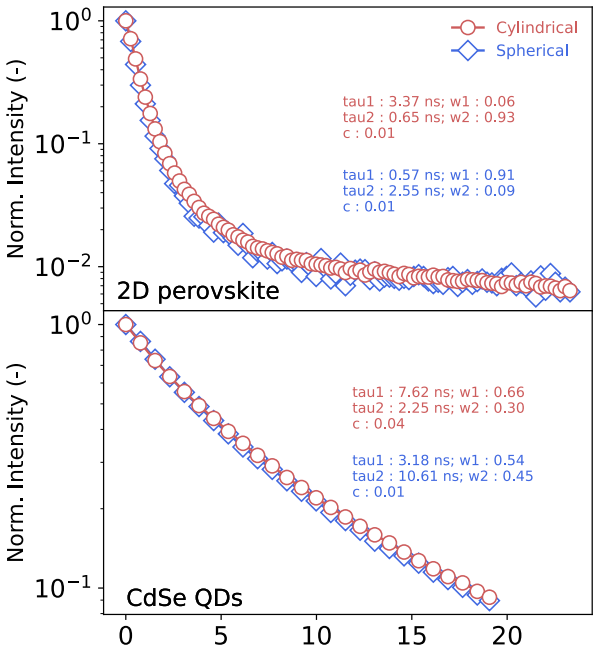

Figure S5. Photoluminescence lifetime decays measured with the cylindrical (red) and the spherical (blue) lenses fitted with a biexponential fit for both the CdSe QDs and 2D perovskites. Fitting parameters are given in the figure.

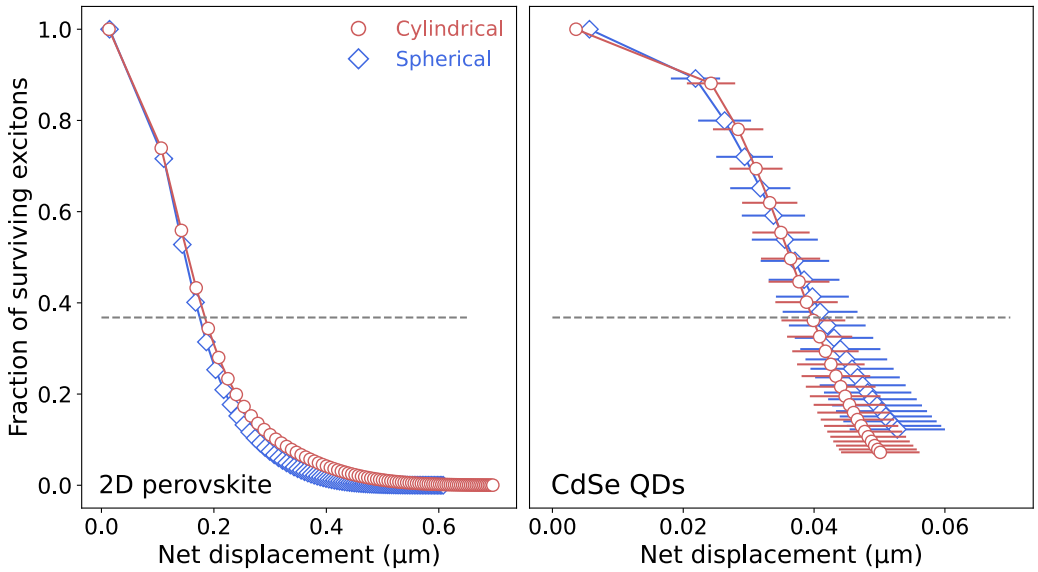

Figure S6. Fraction of surviving excitons (extracted from lifetime data in Supplementary **Figure S5**) as a function of net spatial displacement $\sqrt{MSD(t)}$ for the cylindrical (red) spherical (blue) lenses for both the 2D perovskites and CdSe QDs. Reported errors represent the uncertainty in the fitting procedure for $\sigma(t)^2$. Dashed grey line represents that 1/e of the excitons have survived.

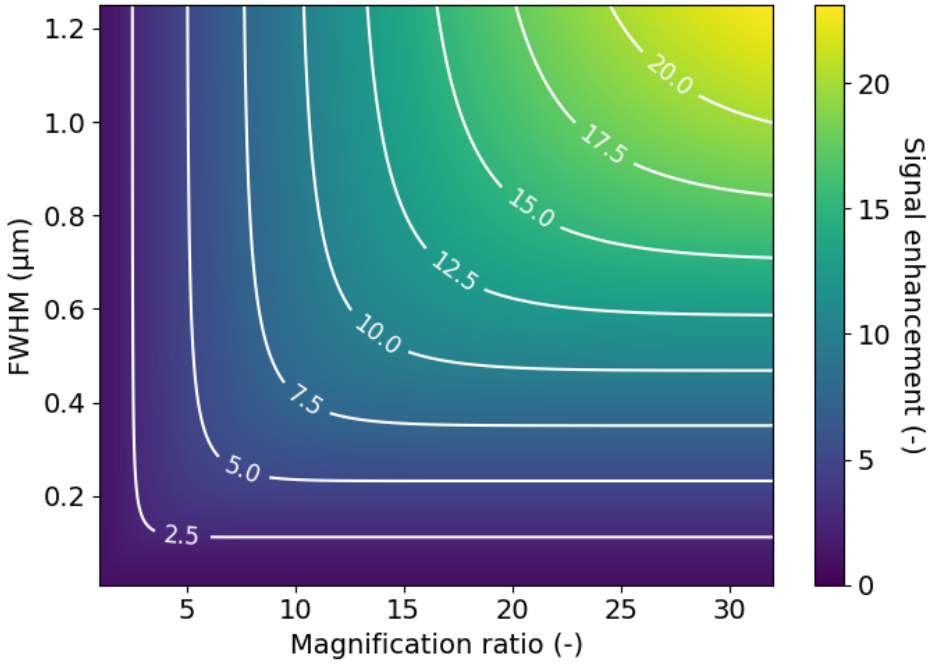

Figure S7. Simulations of the dependence of the signal enhancement (I_{cyl}/I_{sph}) on the magnification ratio (M_y/M_x) and the time- integrated FWHM of the energy carrier population for a detector size of d_0 = 20 μm and y-axis magnification of M_y =400. In similarity with the Voigt distribution, a signal enhancement up to ~25 is predicted for magnification ratios of 30 and FWHM of 1.2 μm. A Gaussian was chosen as population distribution.

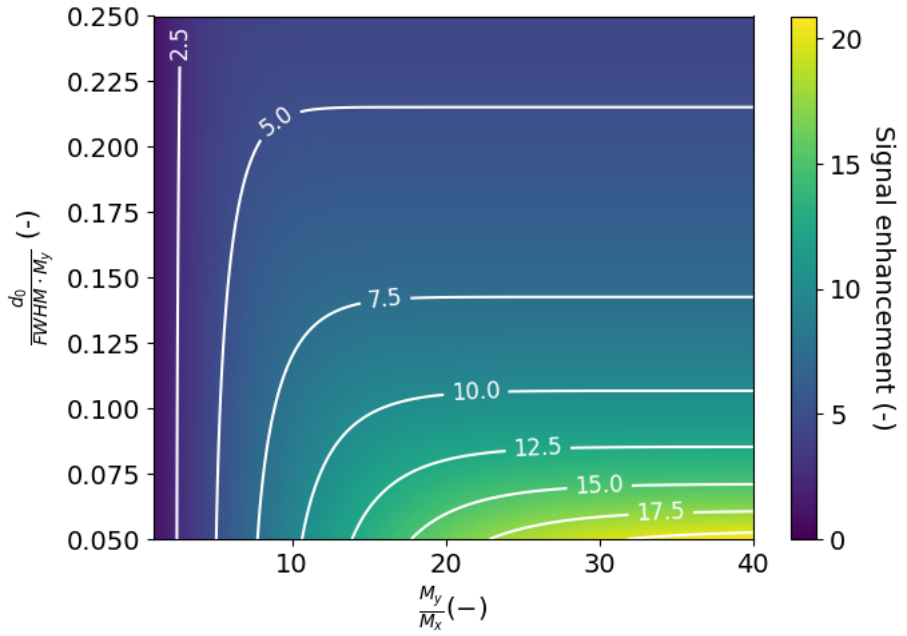

Figure S8 Simulations of the dependence of the signal enhancement (I_{cyl}/I_{sph}) on more general system parameters: d_0 being the detector size, FWHM the population size, and M_y and M_x magnifications in y and x directions, respectively.

References

[1] S. T. Ha, C. Shen, J. Zhang and Q. Xiong, *Nat. Photonics*, 2016, **10**, 115–121.

[2] M. Seitz, P. Gant, A. Castellanos-Gomez and F. Prins, *Nanomaterials*, 2019, **9**(8), 1120

[3] M. Seitz, A. J. Magdaleno, N. Alcázar-Cano, M. Meléndez, T. J. Lubbers, S. W. Walraven, S. Pakdel, E. Prada, R. Delgado-Buscalioni and F. Prins, *Nat. Commun.*, 2020, **11**, 1–8.

[4] F. Prins, D. K. Kim, J. Cui, E. De Leo, L. L. Spiegel, K. M. Mcpeak and D. J. Norris, *Nano Lett.*, 2017, 17, 3, 1319–1325

[5] G. M. Akselrod, F. Prins, L. V. Poulikakos, E. M. Y. Lee, M. C. Weidman, A. J. Mork, A. P. Willard, V. Bulović and W. A. Tisdale, *Nano Lett.*, 2014, **14**, 3556–3562.